

**Assimilation of GBVTD-Retrieved Winds from Single-Doppler Radar for Short-Term
Forecasting of Super Typhoon Saomai (0608) at Landfall**

Kun Zhao^{1,2}, Ming Xue^{2,3} and Wen-Chau Lee⁴

¹Key Laboratory for Mesoscale Severe Weather/MOE and School of Atmospheric Sciences,
Nanjing University, Nanjing, 210093, China

²Center for Analysis and Prediction of Storms and ³School of Meteorology
University of Oklahoma, Norman Oklahoma 73072

⁴Earth Observing Laboratory, National Center for Atmospheric Research*, Boulder, CO
80307

July, 2010

Revised and resubmitted in April 2011

Quarterly Journal of Royal Meteorological Society

Corresponding author address:

Ming Xue

Center for Analysis and Prediction of Storms

University of Oklahoma,

120 David L. Boren Blvd, Norman OK 73072

mxue@ou.edu

*The National Center for Atmospheric Research is sponsored by the National Science Foundation.

Abstract

A single-Doppler wind retrieval method called the Ground-Based Velocity-Track Display technique (GBVTD) has been developed in recent years to retrieve horizontal circulations of tropical cyclones. The technique is able to retrieve axisymmetric tangential and radial winds, asymmetric tangential winds for wavenumbers 1 through 3, and along-beam mean winds in tropical cyclones. It has been successfully applied to tropical cyclone monitoring and warning. This study explores, for the first time, the assimilation of GBVTD-retrieved winds into a tropical cyclone prediction model, and examines its impact relative to that of directly assimilated radial velocity data. Super Typhoon Saomai (2006), the most intense landfalling typhoon ever recorded in China, is chosen as the test case, and data from the coastal operational radar at Wenzhou, China are used. The ARPS 3DVAR system is used to assimilate either the radial velocity data directly or the GBVTD-retrieved winds, at 30-min intervals for 2 hours.

The assimilation of the GBVTD-retrieved winds results in much improved structure and intensity analyses of Saomai compared to those in the Japan Meteorological Agency mesoscale reanalysis as well as that assimilating radial velocity (V_r) data directly. The ability of the GBVTD method in providing wind information covering the full circle of the inner-core circulation is the primary reason for its superior performance over direct assimilation of V_r data; for the latter, the azimuthal data coverage is often incomplete. With the improved initial conditions, the subsequent forecasts of typhoon intensity, track and precipitation are also improved. The improvements to both track and intensity predictions persist over a 12-hour forecast period, which is mostly after landfall. Subjective and quantitative evaluations of the precipitation and circulation patterns show consistent results. A further sensitivity experiment shows that the axisymmetric wind component in the GBVTD retrieval has the dominant impact on the prediction.

1. Introduction

Landfalling tropical cyclone (TC) is one of the most deadly and costly natural hazards; accurate prediction of their track and intensity are crucial for the protection of life and property. Over the past several decades, TC track forecasting has improved steadily due to the increased use of satellite and other observations over the ocean and improved numerical weather prediction (NWP) models. As noted in Elsberry (2005), the prediction of TC track has advanced to the point where the original goals of the U.S. Weather Research Program have been achieved. However, the TC intensity and structure forecasting has improved very slowly (Houze et al. 2007; Davis et al. 2008). One of the main reasons for this slow improvement is the lack of accurate initial conditions that capture the internal structures, including precipitation bands and eyewall, in TCs (Davis et al. 2008).

The Doppler weather radar is the only instrument that can observe the three-dimensional structure of TCs with high spatial and temporal resolutions. For landfalling TCs, coastal Doppler radars often can provide such data coverage near their landfall. A Doppler radar, however, only observes the along-beam component of the 3D wind field. Although dual-Doppler analyses can provide a relatively accurate estimation of the full winds, regions with dual-Doppler coverage are, however, usually rather limited in spatial coverage. As a result, assimilating single Doppler radar data in NWP models remains a primary option where effective assimilation and/or retrieval techniques are necessary. Several recent studies assimilated coastal Doppler radial velocity (V_r) data from multiple radars, using three-dimensional variational (3DVAR) methods (Zhao et al. 2006; Xiao et al. 2007; Zhao et al. 2008b; Zhao and Jin 2008; Zhao and Xue 2009) or ensemble Kalman filter (EnKF) (Zhang et al. 2009; Dong and Xue 2010). While the results are encouraging, assimilating radar data remains a challenging problem and its application to

hurricane prediction is a rather new area of research. With 3DVAR-based methods, the cross-beam components of winds are often not retrieved very well in the absence of dual- or multi-Doppler coverage and the restriction of data to precipitation regions often lead to patchy analysis increments that lack spatial continuity as well as balance among state variables. The EnKF method is theoretically more advanced but its practical application on operational TC forecasts still requires more research.

Traditionally, the initialization of TCs in NWP models often relies on the use of so-called bogus vortex that typically includes an axisymmetric component constructed based on few estimated parameters on TC size and intensity and an asymmetric component extracted from the background fields (Kurihara et al. 1993; Zou and Xiao 2000; Xiao et al. 2009). While proven helpful, the idealization involved in the construction of such vortices has its own problems. The best solution should be to analyze/construct the TC vortex, including its 3D structures, using direct observations as much as possible.

In recent years, a single-Doppler wind retrieval method, called the Ground-Based Velocity-Track Display technique (GBVTD) (Lee et al. 1999, LJCD hereafter), has been developed to retrieve two-dimensional primary circulations of landfalling TCs at different altitudes. GBVTD has been successfully applied to several landfalling TC cases (Lee et al. 2000; Harasti et al. 2004; Lee and Bell 2007; Zhao et al. 2008a) for monitoring and warning purposes. It has been shown that GBVTD is capable of retrieving horizontal winds of mature TCs with an accuracy of about 2 m s^{-1} (Harasti et al. 2004). Lee et al. (2006) derived the divergence and vertical velocities using vorticity equation and high-temporal-resolution GBVTD-retrieved tangential winds in hurricane Danny (1997). In a sense, GBVTD can be considered a more sophisticated vortex-fitting technique that can provide more accurate 3D structures than a typical

bogus vortex does. Assimilating GBVTD-retrieved winds into NWP models for TC forecasting can potentially out-perform commonly used bogus vortex techniques, or even direct assimilation of radial velocity data. This has, however, never been attempted so far, and is the focus of this study.

To build up dynamically consistent TCs from radar observations, an assimilation method that takes advantage of the high temporal and spatial resolutions of the data is necessary. A procedure combining the 3DVAR and complex cloud analysis scheme from the Advanced Regional Prediction System (ARPS, Xue et al. 2003) has proven to be effective in initializing mid-latitude thunderstorms in a number of studies (e.g., Hu et al. 2006, H06 hereafter). Recently, it has been successfully applied to the analysis and forecasting of a landfalling hurricane Ike (2008) in the Gulf of Mexico region of the US (Zhao and Xue 2009). The ARPS 3DVAR (Gao et al. 2004) can analyze either radar radial velocity or radar-retrieved wind data while the cloud analysis procedure determines the cloud and hydrometeor fields from reflectivity (Z) and other cloud observations and adjusts in-cloud moisture and temperature (Brewster 2002; H06).

Encouraged by the above results, this study explores for the first time the assimilation of GBVTD-retrieved winds (V_{GBVTD}) within the ARPS 3DVAR framework for the analysis and prediction of Super Typhoon Saomai (2006), the strongest land-falling typhoon ever recorded in China. During the Saomai's landfall, its inner core region was fully observed by China's Next Radar 1998 Weather Surveillance Doppler (CINRAD WSR-98D) radar located at Wenzhou (WZRD), Zhejiang Province, from 00 to 12 UTC, 10 August 2006, at 6-minute volume scan intervals. The axisymmetric kinematic and dynamic structures of its inner core region were recently examined using GBVTD-retrieved winds from WZRD (Zhao et al. 2008a). In this study, the V_{GBVTD} data are assimilated through 30-min intermittent assimilation cycles during a 2-hour

period before landfall. The impacts of assimilating V_{GBVTD} on the intensity, rainband structure, track and quantitative precipitation prediction of Saomai will be examined, and compared with direct assimilation of radial velocity data, V_r .

This paper is organized as follows. Section 2 describes the assimilation method, domain configuration, model setup and processing of observations. The analysis results are presented and discussed in section 3 while the prediction results in section 4. Summary and conclusions are presented in section 5.

2. Radar data, wind retrieval, and data assimilation

2.1. Radar data processing and quality control

In this paper, full-resolution Level-II data from WZRD are used as the initial input. The WZRD operated in the volume coverage pattern 21 (VCP21) scanning mode of the U.S. WSR-88D standard, which is consisted of 9 elevations starting at 0.5° and ending at 19.5° with a maximum Doppler range of 150 km. With large volumes of radar observations that are recorded at a higher resolution than the forecast model grid spacing (3 km in horizontal in this study), data thinning and careful quality control of the observations become necessary. For quality control, we first use the quality control procedures within the 88d2arps program available in the ARPS system (Brewster et al. 2005) to remove/correct erroneous observations, including velocity dealiasing and ground clutter removal. As described in Brewster et al. (2005), the velocity unfolding utilizes a horizontal mean profile derived from an analysis background to estimate the gate-to-gate shear due to mean vertical shear, and check the derivations in the data from this shear for folding problems. Several additional steps are involved in performing the velocity unfolding. After the automatic quality control is performed, the data are further examined and edited manually when necessary using the interactive “SOLO” software (Oye et al. 1995) from

NCAR. The final V_r data are then remapped to the model grid points using a local least square fitting method for use by the 3DVAR analysis; for the GBVTD wind retrieval they are interpolated onto constant-altitude plan position indicators (CAPPIs) in Cartesian coordinates instead.

2.2. GBVTD wind retrieval

The GBVTD technique (LJCD) represents a modification to a fixed-coordinate-system velocity track display (VTD) technique originally proposed by Lee et al. (1994); the latter tries to deduce properties of the primary circulations of tropical cyclones from airborne Doppler radar data. Formulated upon a cylindrical coordinate system centered at the TC circulation center, the GBVTD analysis uses the Doppler velocities along a constant radius to deduce the tangential and radial winds of a vortex via Fourier decomposition, in a way similar to the velocity azimuth display (VAD) technique (Browning and Wexler 1968). In this study, the V_{GBVTD} data are very similar to those produced in Zhao et al. (2008a). The domain of the GBVTD analyses extends from the center of the typhoon to an 80 km radius and from 1 to 10 km in the vertical. Grid spacing is 1 km in the radial and vertical directions, and 4 degrees in the azimuthal direction. Missing data below 2 km height are extrapolated from above using the same method as Lee et al. (2006). It is worth pointing out that the extrapolation may not capture the realistic variation of the boundary layer wind profile, thus affecting the low-level wind analysis. Quantities, including the component of mean wind in the direction from the radar to typhoon center, $V_{M\parallel}$, the axisymmetric tangential wind, V_{T0} , the axisymmetric radial wind, V_{R0} , and the asymmetric tangential winds for different wavenumbers, V_{Tn} , ($n = 1, 2, 3$) are deduced by the GBVTD analysis. As pointed out by LJCD, the maximum wavenumber resolved at each radius varies with the maximum angular data gap; for data having gaps of 30° , 60° , 120° , and 180° , the maximum

wavenumbers resolved are 3, 2, 1, and 0, respectively. In addition, the unresolved asymmetric radial wind is aliased into the asymmetric tangential winds (LJCD). The unresolved mean wind component perpendicular to $V_{M\parallel}, V_{M\perp}$, is approximated by the storm motion vector in the direction of $V_{M\perp}$ (Harasti et al. 2004) and is used to wind correct V_{T0} . The total GBVTD winds, V_{GBVTD} , contain all components, $V_{M\parallel}, V_{M\perp}, V_{T0}, V_{R0}$, and V_{Tn} ($n=1, 2$, and 3), unless stated otherwise.

2.3. The ARPS and ARPS 3DVAR

The non-hydrostatic ARPS prediction model with full physics is used during the assimilation cycles and for the follow-on forecast. The physics options used include the Lin ice microphysics, Goddard long and shortwave radiation, a 2-layer soil model and the TKE-based subgrid-scale turbulence and PBL parameterization (see Xue et al. 2001 for details). A $611 \times 611 \times 53$ grid at 3-km horizontal grid spacing is used (Fig. 1). The domain depth is 25 km and the near-surface vertical grid spacing is about 50 m. Initial analysis and lateral boundary conditions (LBCs) for the ARPS model are from the Japan Meteorological Agency (JMA) 6-hourly gridded regional analyses at 20-km horizontal resolution with 20 pressure levels. The JMA analyses were produced using a multivariate three-dimensional (3D) optimum interpolation (OI) method to combine first-guess fields from JMA's regional spectral model (RSM) with observations from a variety of platforms (Segami et al. 1989; Onogi 1998; Tsuyuki and Fujita 2002).

The ARPS 3DVAR uses an incremental form of the cost function that includes the background, observation, and mass-continuity equation constraint terms. The analysis variables include the three wind components, potential temperature, pressure, and water vapor mixing ratio (Gao et al. 2004). In the current system, the cross-correlations between variables are not included in the background error covariance. The spatial covariance of background error is

assumed spatially homogeneous and Gaussian, and is modeled using a recursive filter. The observation errors are assumed to be uncorrelated so that the observation error covariance matrix is diagonal, and its diagonal elements are specified according to the estimated observation errors. The standard derivations of the observational errors are prescribed to be 1.5 ms^{-1} and 3 ms^{-1} for V_r and V_{GBVTD} data based on the statistics of data samples. For the radar data, a 10 km horizontal and 4 grids vertical covariance de-correlation scales are used in the 3DVAR.

2.4. Experimental design

All forecasts use their final analysis at 0600 UTC 10 August 2006 as the initial condition and run for 12 hours, which cover the landfall and post-landfall periods of Saomai. The baseline control forecast without radar data assimilation (CNTL) starts the forecast from the 0600 UTC 10 August JMA reanalysis. Experiments ExpGV and ExpVr, which assimilate the V_{GBVTD} and V_r data, respectively (see Table 1), are designed to examine the impacts of assimilating V_{GBVTD} versus V_r data. The data assimilation goes from 0400 to 0600 UTC at 30 minute intervals. Before 0400 UTC, there is a 4-hour pre-forecast period starting from the 0000 UTC JMA reanalysis. To further evaluate the relative importance of the asymmetric component in the GBVTD retrieval, one additional experiment, called ExpGVNoAsy, is performed in which the asymmetric component is excluded.

3. Results of GBVTD retrieval and data assimilation

3.1. Performance of GBVTD retrieval

To assess the quality of the retrieved velocity, V_{GBVTD} , the root-mean-square error (RMSE) between the V_r re-sampled from V_{GBVTD} and the V_r observed by WZRD radar is calculated at various heights from 0400 and 0600 UTC (Fig. 2). It is found that the V_r re-sampled from V_{GBVTD}

are consistent and in good agreement with the observed V_r during the analysis period, with RMSEs between 1 and 2 m s⁻¹, well below the observation error of 3 m s⁻¹ assumed in ARPS3DVAR analysis. The maximum RMSE of ~ 1.8 m s⁻¹ is found at 0400 UTC when the center of Saomai just entered the Doppler range of WZRD. The RMSEs decrease to about 1.2 m s⁻¹ around 0600 UTC as more circulation of Saomai is observed by WZRD.

The retrieved V_{GBVTD} field together with the observed reflectivity Z , the observed V_r , and the re-sampled V_r from V_{GBVTD} at 3 km height at 0400 (the first analysis time) and 0600 UTC (the final analysis time) are shown in Fig. 3. At 0400 UTC, the center of Saomai just entered the coverage of WZRD when the eyewall is located at radius $R \approx 18$ km, with an organized outer rainband at $R \approx 60$ km (Fig. 3a). The WZRD V_r field shows a clear dipole velocity signature associated with the eyewall, but the far side of the eyewall is outside the Doppler range (Fig. 3c). In comparison to the observed V_r , V_{GBVTD} not only recovers the cross-beam typhoon circulation, it also fills the regions where V_r data are missing (Fig. 3a). It thereby provides an estimate of the full vortex circulation within an 80 km radius of the typhoon center. In addition, the V_{GBVTD} field reveals a distinct asymmetric wavenumber one structure with high wind speeds located northwest of the typhoon center, collocated with the high reflectivity regions associated with both the eyewall and an outer rainband. The pattern of V_r re-sampled from V_{GBVTD} is close to the observed V_r , with an RMSE of about 1.5 m s⁻¹ (Fig. 3e), indicating that the observed radial wind information has been retained rather accurately in V_{GBVTD} .

By 0600 UTC, Saomai has formed a concentric eyewall structure as its outer rainband evolves into the outer eyewall (Fig. 3b). Two dipoles are observed in the WZRD V_r field, corresponding to the inner and outer eyewalls, respectively (Fig. 3d). The V_{GBVTD} data describe

the concentric eyewall feature and the complete inner-core vortex circulation better than the WZRD V_r observations (Fig. 3b and Fig. 3c).

3.2. Assimilation of GBVTD-retrieved winds versus V_r data

Fig. 4 shows the horizontal winds of Saomai at $Z = 3$ km from the 4-hour forecast starting from the JMA reanalysis at 0000 UTC (Fig. 4a), which is the background of the first 3DVAR analysis for all assimilation experiments. The figure also shows the results of first analysis from experiments ExpVr (Fig. 4b) and ExpGV (Fig. 4c). The typhoon in the background forecast shows a broad eye with an eyewall radius of about 100 km. After V_r or V_{GBVTD} data are assimilated once at 0400 UTC, in ExpVr and ExpGV respectively, the eyewall radius is reduced to ~ 30 km and ~ 20 km respectively, and the vortex circulation in the inner core region is strengthened with a clear wavenumber one asymmetry pattern (Figs. 4b and 4c. v.s. Fig. 4a). The high wind speed is located at the northeast quadrant of the vortex with the maximum increasing to about 65 m s^{-1} in ExpGV (Fig. 4b) and 60 m s^{-1} in ExpVr (Fig. 4c), compared to about 48 m s^{-1} in the background forecast (Fig. 4a). It is clear that assimilating either V_r or V_{GBVTD} significantly improves the structural details as well as the intensity of the typhoon.

It is interesting to note that major structure differences exist already between the analyses of ExpVr (Fig. 4b) and ExpGV (Fig. 4c), after only one analysis at 0400 UTC. First, the shape of the eyewall is elliptical in ExpVr compared to the more circular shape in ExpGV. The major axis of the ellipse in ExpVr is along the direction connecting the radar and typhoon center. The horizontal winds in ExpVr are obviously weaker than those in ExpGV at the northwest and southeast quadrants of typhoon along the major axis of the ellipse. In ExpVr, it is evident that the total wind field (Fig. 4b) is very close to the observed V_r field, in magnitude and structure (Fig. 3c), showing that the cross-beam wind component is mostly missing in the 3DVAR analysis

from single-Doppler V_r data in this case. A similar situation was reported in Li et al. (2010). In contrast, assimilating V_{GBVTD} data produces a more realistic analysis.

Fig. 5 shows the mean sea level pressure (MSLP) and surface wind speed from CNTL (JMA analysis), ExpVr and ExpGV at the end of the data assimilation window (0600 UTC). Clearly, the typhoon intensity in the JMA analysis is too weak (Fig. 5a); its MSLP is about 989 hPa versus 920 hPa in the best track data. In this study, the best track data are provided by the Shanghai Typhoon Research Institute of Chinese Meteorological Administration (Yu 2007; Song et al. 2010). The best track maximum surface wind (MSW) is about 61 m s^{-1} , while that in CNTL is only about 29 m s^{-1} . The typhoon is significantly deeper in ExpGV and ExpVr, with their MSLP being 934 and 950 hPa, respectively. The typhoon circulation in ExpGV is also the strongest, consistent with the lower MSLP. The horizontal wind speeds in both ExpGV and ExpVr exhibit wavenumber one asymmetry with similar MSW, but the locations of their peak winds are different. The high wind area in ExpGV is located in the northwest quadrant of the vortex, closer to the radar observations (not shown); in ExpVr, the high wind area is located in the southwest quadrant instead. Besides the improvement in intensity, the analyzed typhoon centers are closer to the observed locations with radar data assimilation. The center location improvement is most evident in ExpGV; the observed center location is indicated by a black dot in Fig. 5.

To examine the vertical structure of the analyzed typhoon, east-west vertical cross sections of horizontal wind speed through the typhoon center are presented in Fig.6 for CNTL, ExpVr and ExpGV. In CNTL, the weak vortex circulation and the large eye are evident (Fig. 6a). The vortex in ExpVr (Fig. 6b) is much stronger with a more upright eyewall than in CNTL.

Assimilating V_{GBVTD} data in ExpGV (Fig. 6c) results in an even more upright eyewall and the strong tangential winds extend to a much higher level than in ExpVr (Fig. 6b).

To compare the axisymmetric structures, the azimuthal mean tangential winds of the analyzed typhoons are plotted in Fig. 7; again the vortex circulation is much weaker is much weaker and broader in CNTL (Fig. 7a) while that in ExpGV is the strongest. The vortex in ExpVr (Fig. 7b) has a radius of maximum wind (RMW) of about 30 km, close to the best track value of about 20 km; a 49 m s^{-1} maximum tangential wind is found below 1.5 km. In ExpGV (Fig. 7c), the vortex has a smaller RMW of about 20 km, and a maximum mean wind speed of about 55 m s^{-1} . It is also noted that a secondary wind maximum is found at a radius of about 55 km in ExpGV (Fig. 7c), which is associated with the outer eyewall; such a secondary maximum is not found in ExpVr. Although the vertical structure cannot be directly verified by observations, the steepest slope of the RMW line associated with the smallest RMW in ExpGV is consistent with the study of Stern and Nolan (2009), where the slope of the RMW is found to be inversely proportional to the RMW. The more realistic vortex structure obtained in ExpGV can be attributed to a better representation of the vortex inner core circulation by the V_{GBVTD} wind data.

4. Forecast results

4.1. Impact of wind assimilation on typhoon structure forecast

We first examine the impact of assimilating V_{GBVTD} or V_r data on the predicted structure of Saomai (2006). Fig. 8 shows the composite (column maximum) radar reflectivity and 3-km height wind fields at 3, 6, 9 and 12 hours of forecast from experiments CNTL, ExpVr, and ExpGV, as compared to the corresponding reflectivity observations in the first row. At 0900 UTC, the 3-hour forecast time, the predicted vortex in CNTL (Fig. 8e) continues to be weaker and broader than that in other experiments. The reflectivity is over-predicted in CNTL in a

spurious rainband on the northwest side of the vortex (Fig. 8e). We note that CNTL was able to quickly spin up precipitation within the first 1 to 2 hours of forecast, even though its initial condition from the GFS did not contain any hydrometeor. In comparison, the 3-hour forecasts of the radar-assimilating experiments, ExpGV and ExpVr (Fig. 8i and Fig. 8m) show tighter vortex circulations and rainbands located closer to the vortex center.

By 1200 UTC, the 6-hour forecast time, Saomai had moved over land. The typhoon center is now filled with precipitation after landfall, and the strong echo regions ($Z > 40$ dBZ) are now in the northeast and southeast quadrants of the typhoon (Fig. 8b). Saomai's center in all three experiments had also made landfall by this time. The center in ExpGV (Fig. 8n) appears to be best positioned, while Saomai's motion in CNTL (ExpVr) appears faster (slower) than that in the best track data (Fig. 8f and Fig. 8j). The predicted reflectivity structure in CNTL continues to exhibit broad spiral rainband structures and the center of the vortex has a large weak reflectivity hole. In ExpVr, most of the strong reflectivity (> 35 dBZ) is still offshore, inconsistent with radar observations, while in ExpGV, the strong reflectivity is mostly over land and confined to a small region near the vortex center, as observed.

At the 9 hours of forecast, the precipitation pattern became more asymmetric (Fig. 8c). The observed strong precipitation is now mostly located in the southeast half of the vortex, presumably due to the stronger moisture transport from the ocean on the southeast side, and some interaction with the terrain in Zhejiang Province (Saomai made landfall at the border of Zhejiang and Fujian Provinces shown in Fig. 1). On the west side of the vortex, there should be entrainment of drier air from the higher latitudes that tends to suppress precipitation.

The observed reflectivity structure is best captured by ExpGV. Both the reflectivity pattern and the position of strong reflectivity in the vortex agree very well with observations (Fig. 8o).

The reflectivity in CNTL remains rather broad and becomes disorganized (Fig. 8g). The reflectivity pattern in ExpVr is closer to observations than CNTL but most of the high reflectivity is found in the eastern half of the vortex rather than on the southeast side. It also exhibits two rainbands within the high reflectivity region which are not observed (Fig. 8k). The vortex circulations in ExpGV and ExpVr still appear tighter than in CNTL.

At the 12 hours of forecast, the precipitation is completely over land and the strong echo region remains concentrated in the southeast quadrant as earlier. Again, the forecast of ExpGV has the best agreement with observations (Fig. 8p), while that of CNTL has the worst agreement (Fig. 8h). The vortex in CNTL is rather broad while its precipitation region is significantly off centered.

To better compare the structure and intensity among these experiments, the MSLP and surface wind speed at 0900 UTC 10 August (3-hour forecast time) when the typhoon is near landfall are shown in Fig. 9. It is clear that the forecast vortices in ExpGV and ExpVr are much more intense than that in CNTL, and the 948 hPa minimum MSLP in ExpGV is closest to the best track MSLP of 935hPa. CNTL only predicted a 988 hPa MSLP with the strongest winds found at about 70 km from the center. It is noted that the surface wind speeds from both radar-assimilating experiments exhibit a wavenumber-1 asymmetry, but their locations of peak winds are different. The high wind speeds in ExpGV are located in the north-northeast quadrant, while those in ExpVr are mostly in the eastern quadrant. In addition, the predicted typhoon center in ExpGV is closer to the best track location (black dot) than those in CNTL and ExpVr.

South-north cross sections of equivalent potential temperature (θ_e) and horizontal wind speed through the predicted typhoon center at hour 3 are plotted in Fig. 10 for CNTL, ExpVr and ExpGV. Consistent with results shown in Fig. 9, the typhoon is weaker with a very large eye in

CNTL. Compared to CNTL (Fig. 10a), the typhoon inner core in ExpVr (Fig. 10b) and ExpGV (Fig. 10c) is much better defined, with the narrow eye region extending vertically from surface to about 7-8 km height before expanding in diameter. High θ_e values are found in the eye region, indicating air of upper level origin due to descent within the eye. High θ_e values are also found in the boundary layer. The low-level θ_e contours turn upward, with an outward slope that more or less follows the axis of maximum winds. Consistent with Fig. 10, the azimuthal mean tangential wind and the horizontal temperature anomaly (defined at each level as the deviation from the temperature averaged over a horizontal area within a radius of 180 km, similar to Liu et al. (1999)) at this time also reveal an enhanced vortex in the forecasts of ExpVr (Fig. 11a) and ExpGV (Fig. 11b), accompanied with a clear warm-core in the eye region. The maximum temperature anomaly is at about 7 km height, similar to those found in previous observations and simulations of intense TCs (Hawkins and Imbembo 1976; Liu et al. 1999). Wind speeds higher than 35 m s^{-1} extend to nearly 7 km height in ExpGV, higher than in ExpVr; the wind speed decreases rapidly above 7 km, consistent with the level of maximum temperature anomaly and the expected cyclostrophic balance. The maximum of warm core anomaly is about 16 K in ExpGV, higher than that in ExpVr. These features are consistent with the fact that ExpGV predicts a stronger typhoon than ExpVr. It is noted the maximum azimuthal mean wind below 1 km in ExpGV is slightly weaker than that in ExpVr, which can be attributed to the earlier landfall in ExpGV.

Overall, the radar-assimilating experiments have shown better predictions of the circulation and precipitation structures in Saomai up to the 12 hours of forecast. The forecast assimilating V_{GBVTD} data is better than that assimilating V_r data.

4.2. Track and intensity predictions

The predicted typhoon track, MSW and MSLP from CNTL, ExpVr, and ExpGV are plotted in Fig. 12 together with the best track data for the 12-hour forecast period from 0600 UTC to 1800 UTC 10 August 2006. Fig. 12a shows the predicted and observed tracks, while Fig. 12b shows the track errors (in km) at each forecast hour. In CNTL, the predicted typhoon track has a northwestward bias (Fig. 12a), resulting in a 12-hour mean error of about 36 km (Fig. 12b). In comparison, the 12-hour mean track error is reduced to 21 and 23 km in ExpVr and ExpGV (Fig. 12b), respectively. In the first 4 hours of forecast, ExpGV shows the closest track to observations, presumably due to its best analysis of the initial storm structure and location as indicated in Fig. 5. After that time, the track error of ExpVr becomes the smallest among the three experiments. Such a switch in relative predicted track errors between ExpGV and ExpVr can be explained from their initial difference. As shown in Fig. 5, there is a southward deviation of the vortex center in the initial field of ExpVr, which happens to offset the northward deviation of track during later forecasts, considering both ExpGV and ExpVr have a tendency of northward track forecast bias. Apparently, even though the radar data assimilated in this study cannot influence the large-scale environment, the assimilation of either V_{GBVTD} or V_r data does have a positive impact on the track forecasts, mainly through initializing a vortex with more realistic intensity and structure. Fovell et al. (2009) showed that the structure differences in simulated TCs can influence their motion within the same large-scale environment. The ‘beta gyre’ effect was quoted as the primary mechanism.

The best-track MSLP and MSW and those predicted by CNTL, ExpVr and ExpGV are plotted in Fig. 12c and Fig. 12d, respectively. Clearly, CNTL significantly under-predicts the intensity in terms of both MSLP and MSW, mainly due to a weaker intensity in the initial

condition. The radar-assimilating experiments show a notable improvement in intensity forecast. ExpGV shows an even better intensity forecast than ExpVr in terms of MSLP (Fig. 12c) while the MSW is about the same in the final analyses and forecasts between the two experiments (Fig. 12d). This again suggests that the assimilation of V_{GBVTD} data is more effective in improving the intensity of the overall vortex.

It is noted that the differences in MSLP among all assimilation experiments are largest at the initial time. By 8 h, the difference between ExpGV and ExpVr becomes rather small (although their MSLPs are still significantly lower than that of CNTL). This can be attributed to the rapid filling of Typhoon Saomai after landfall. As low-pressure anomaly decreases in all experiments, the MSLP differences also decrease. Similar trend was found in a landfalling hurricane Ike (Zhao and Xue 2009). The intensity in terms of MSW shows similar weakening trend, but the MSW in ExpVr decreases more slowly, particularly between 4 ~7 hours (Fig. 12d). This can be attributed to the time lag in storm landfall in ExpVr compared to other experiments, which somewhat delays the vortex filling.

4.3. Precipitation forecasting

Inland flooding is the biggest hazard of landfalling TCs. Accurate precipitation forecast is therefore very important. Fig. 13 compares the total accumulated precipitation during the 12-hour forecast period from the three experiments against high-resolution Automatic Weather Station rainfall observations (Fig. 13a). It is clear that CNTL (Fig. 13b) significantly underestimates the accumulated precipitation over land (where rainfall observations are available), along the path of the inner-core region. The observed precipitation shows a maximum near 27.5° N, close to WZRD radar (indicated by the black arrow in Fig. 13a), and a band of strong precipitation along the border of Zhejiang and Fujian Provinces (c.f., Fig. 1). Compared

with CNTL (Fig. 13b), the two radar-assimilating experiments show clear improvements in 12-hour precipitation forecast. The strong rainband north of the provincial border with a maximum reflectivity near WZRD is well captured, although the precipitation maximum south of the border is still underestimated in both experiments. Assimilating V_{GBVTD} data in ExpGV enhances the precipitation left of the storm track in northern Fujian (Fig. 13d) more than that in ExpVr (Fig. 13c). For lighter precipitation, the general pattern is similar to the available observations in all experiments.

For quantitative evaluation, equitable threat scores [ETS, also called Gilbert Skill Score, Schaefer (1990)] and biases of the 12-hour accumulated precipitation forecasts are plotted in Fig. 14 as a function of precipitation thresholds for all three experiments. It is immediately clear that the radar-assimilating experiments obtain higher ETS scores than CNTL. Among them, ExpGV has the highest ETS scores for almost all thresholds; it also has the least precipitation bias, with the bias being close to one for thresholds between 0 and 200 mm. CNTL over-predicts the weak precipitation and under-predicts heavy precipitation, consistent with a weaker predicted typhoon. Its ETS scores drop quickly above the 50 mm threshold. ExpVr under-predicts the precipitation for all except the smallest thresholds (< 20 mm). These quantitative scores again indicate that assimilating V_{GBVTD} data is most effective while assimilating V_r data directly is also helpful, though to a lesser extent.

In addition to ETS scores for the accumulated precipitation, we also calculated the ETS scores for instantaneous composite (column maximum) radar reflectivity at 20 dBZ and 40 dBZ thresholds and for different forecast ranges (Fig. 15). The composite reflectivity fields were constructed from level-II data from multiple radars, some of which were shown earlier in Fig. 8. For the 20 dBZ threshold (Fig. 15a), CNTL has slightly higher scores at hours 2 and 3 among all

experiments, but its scores become the lowest afterwards. ExpGV and ExpVr have similar scores before hour 4. The scores of ExpGV then steadily increase and remain significantly above those of CNTL and ExpVr afterwards. Its scores are about 0.5 between 7 and 12 hours, which are rather high values for high-resolution instantaneous reflectivity fields. For the 40 dBZ threshold (Fig. 15b), CNTL has the lowest scores for all thresholds, while the scores of ExpGV are consistently the highest. The scores of ExpVr are roughly halfway between those of ExpGV and CNTL. These scores indicate that the assimilation of radar data improves heavy precipitation even more, with the assimilation of GBVTD data being more effective. These quantitative results are in agreement with our earlier subjective assessment.

4.4. Role of the axis-asymmetric component of GBVTD retrieval

Past studies have shown the importance of asymmetry on tropical cyclone propagation and evolution (e.g., Wu and Wang 2000, 2001). To evaluate the relative importance of the GBVTD-derived axisymmetric versus asymmetric wind components in data assimilation, we perform one additional experiment in which the asymmetric components are excluded from the retrieval. Basically we want to assess how important are the structures above wavenumber zero in the retrieval. We call this experiment, ExpGVNoAsy. For brevity, we mainly present predicted track and intensity of this experiment in Fig. 12. As shown, the predicted track and intensity in ExpGVNoAsy remain very close to those in ExpGV, suggesting that the axisymmetric wind component has a dominant role in improving the track and intensity forecasting in this case. We do note here that this conclusion may be case dependent, and more cases are needed to draw more definite or statistical conclusions.

5. Summary and conclusions

This study explores, for the first time, the assimilation of GBVTD-retrieved winds into a numerical weather prediction model running at a 3-km horizontal resolution for the analysis and forecasting of Super Typhoon Saomai (2006), the strongest land-falling typhoon ever recorded in the offshore region of Mainland China. The GBVTD-retrieved winds from the radial velocity data or the radial velocity data from single coastal operational weather radar at Wenzhou, Zhejiang Province, China were assimilated over a 2-hour period prior to landfall; the ARPS 3DVAR/cloud analysis system was used with 30-min assimilation cycles. Twelve-hour-long predictions were made from the final analyses. The results suggest the followings:

The assimilation of GBVTD-retrieved winds (V_{GBVTD}) in experiment ExpGV results in much improved structure and intensity analyses over a control forecast initialized directly from the JMA (Japan Meteorological Agency) mesoscale reanalysis, as well as over experiment ExpVr that assimilates radial velocity (V_r) data directly. The ability of the GBVTD-based method in determining the full circle of vortex circulation in the inner-core region is the primary reason for ExpGV to outperform ExpVr with direct V_r assimilation. The GBVTD-retrieved winds have the advantages of not only providing the cross-beam wind component but also filling in data void regions when precipitation is unevenly distributed in the inner core region. With the improvement in the initial conditions, the subsequent forecasts of typhoon intensity, track and precipitation are also improved. The improvements to both track and intensity predictions persist over the 12 hour forecast period, which is mostly after landfall. The subjective evaluations of the precipitation and circulation patterns and quantitative evaluations of precipitation and reflectivity against observations also support these findings. A further sensitivity experiment shows that the axisymmetric wind component in the GBVTD retrieval has a dominant impact on the prediction.

Although our conclusions here are based on a single land-falling typhoon case, the impact of V_{GBVTD} data on the structure, intensity, track and precipitation forecast of landfalling typhoon is promising as long as enough radar data coverage is available for successful wind retrieval from the GBVTD algorithm. In fact, we have obtained preliminary results applying this method to hurricane Ike (2008) studied by Zhao and Xue (2009) and the results are consistent with the findings here. Furthermore, our algorithm should be applicable to airborne radar data too, and therefore has the potential to improve tropical cyclone forecasts long before landfall. Work along this line is underway. Finally we point out again the GBVTD retrieval can be considered a much more sophisticated procedure for building a ‘bogus’ vortex. It directly use radar wind observations, and tries to build a three dimensional vortex that contains axis-asymmetric circulations up to wave number 3 that best fit the radar observations while traditional bogus vortex usually employs much simpler vortex models. As the GBVTD retrieval including quality control is computationally very fast; it can be completed within one minute using a current-generation single-processor in Linux computer, it can be used in real time without much increase in the analysis cost. We also note that the GBVTD retrieval can be assimilated into the numerical model using more sophisticated data assimilation methods, such as 4DVAR (e.g., Zou and Xiao 2000) and ensemble Kalman filter. In the latter case, dynamically more consistent pressure and temperature fields are expected; in our current case using 3DVAR for the wind analysis, we rely on frequent assimilation cycles to spin up other fields. In the future, we plan to compare our GBVTD procedure against bogus-vortex methods, and test the algorithms using more cases to more robust conclusions.

Acknowledgement: This work was supported by NSF grants AGS-0802888, OCI-0905040, and funding from OU VPR Office, Office of Naval Researching grant N00014-10-1-013, N00014-

10-1-0775, the National Natural Science Foundation of China (grants 40975011 and 40505004), the Social Commonwealth Research Program (GYHY201006007), the National Grand Fundamental Research 973 Program (2009CB421502), and the National Thousand People Plan. We would also like to acknowledge the China Meteorological Administration for collecting and archiving the radar data used in this study. K. Brewster provided assistance for the quality control of radar data. Y. Wang, J. Gao, G. Ge, N. Du, K. Zhu and Q. Wang are thanked for helps with ARPS and ARPS3DVAR. Supercomputers at TACC, University of Texas, and at OSCER, University of Oklahoma were used.

References

- Brewster K, 2002: Recent advances in the diabatic initialization of a non-hydrostatic numerical model. *Preprints, 15th Conf Num. Wea. Pred./ 21st Conf Severe Local Storms*, San Antonio, TX, Amer. Meteor. Soc., J6.3.
- Brewster K, Hu M, Xue M, Gao J, 2005: Efficient assimilation of radar data at high resolution for short-range numerical weather prediction. *WWRP Int. Symp. Nowcasting Very Short Range Forecasting*, CDROM 3.06.
- Browning KA, Wexler R, 1968. A determination of kinematic properties of a wind field using Doppler radar. *J. Appl. Meteor.*, **7**: 105-113.
- Davis C, Wang W, Chen SS, Chen YS, Corbosiero K, DeMaria M, Dudhia J, Holland G, Klemp J, Michalakes J, Reeves H, Rotunno R, Snyder C, Xiao QN, 2008. Prediction of landfalling hurricanes with the Advanced Hurricane WRF model. *Monthly Weather Review*, **136**: 1990-2005.
- Dong J, Xue M, 2010: Ensemble Kalman filter assimilation of coastal WSR-88D radar data and forecasting for hurricane Ike (2008). *29th Conf. Hurricanes Tropical Meteor.*, Tucson, AZ, Amer. Meteor. Soc., Paper No. P2.138.
- Elsberry RL, 2005. Achievement of USWRP hurricane landfall research goal. *Bull. Amer. Meteor. Soc.*, **86**: 643-645.

- Fovell RG, Corbosiero KL, Kuo H-C, 2009. Cloud microphysics impact on hurricane track as revealed in idealized experiments. *J. Atm. Sci.*: 1764-1778.
- Gao J-D, Xue M, Brewster K, Droegemeier KK, 2004. A three-dimensional variational data analysis method with recursive filter for Doppler radars. *J. Atmos. Ocean. Tech.*, **21**: 457-469.
- Harasti PR, McAdie CJ, Dodge PP, Lee W-C, Tuttle J, Murillo ST, Marks FD, 2004. Real-Time Implementation of Single-Doppler Radar Analysis Methods for Tropical Cyclones: Algorithm Improvements and Use with WSR-88D Display Data. *Weather and Forecasting*, **19**: 219-239.
- Hawkins HF, Imbembo SM, 1976. The structure of a small, intense hurricane-Inez 1966. *Mon. Wea. Rev.*, **104**: 418-442.
- Houze RA, Jr., Chen SS, Smull BF, Lee W-C, Bell MM, 2007. Hurricane intensity and eyewall replacement. *Science*, **315**: 1235-1239.
- Hu M, Xue M, Brewster K, 2006. 3DVAR and cloud analysis with WSR-88D level-II data for the prediction of Fort Worth tornadic thunderstorms. Part I: Cloud analysis and its impact. *Mon. Wea. Rev.*, **134**: 675-698.
- Kurihara Y, Bender MA, Ross RJ, 1993. An initialization scheme of hurricane models by vortex specification. *Mon. Wea. Rev.*, **121**: 2030-2045.

- Lee JL, Lee W-C, MacDonald AE, 2006. Estimating vertical velocity and radial flow from Doppler radar observations of tropical cyclones. *Q J Roy Meteor Soc*, **132**: 125-145.
- Lee W-C, Jr. FDM, Carbone RE, 1994. Velocity track display (VTD)-A technique to extract real-time tropical cyclone circulation using a single airborne Doppler radar. *J. Atmos. Oceanic. Technol.*, **11**: 337-356.
- Lee W-C, Jou BJD, Marks Jr FD, 2000. Tropical Cyclone Kinematic Structure Retrieved from Single-Doppler Radar Observations. Part III: Evolution and Structures of Typhoon Alex (1987). *Mon. Wea. Rev.*, **128**: 3982.
- Lee W-C, Jou BJ-D, Chang P-L, Deng S-M, 1999. Tropical Cyclone Kinematic Structure Retrieved from Single-Doppler Radar Observations. Part I: Interpretation of Doppler Velocity Patterns and the GBVTD Technique. *Mon. Wea. Rev.*, **127**: 2419-2439.
- Lee W-C, Bell MM, 2007. Rapid intensification, eyewall contraction, and breakdown of Hurricane Charley (2004) near landfall. *Geophys. Res. Lett.*, **34**: L02802, doi:10.1029/2006GL027889.
- Li W, Xie Y, Deng S-M, Wang Q, 2010. Application of the Multigrid Method to the Two-Dimensional Doppler Radar Radial Velocity Data Assimilation. *J. Atmos. Ocean. Tech.*, **27**: 319-332.

- Liu Y, Zhang D-L, Yau MK, 1999. A Multiscale Numerical Study of Hurricane Andrew (1992).
Part II: Kinematics and Inner-Core Structures. *Mon. Wea. Rev.*, **127**: 2597-2616.
- Onogi K, 1998. A data quality control method using forecasted horizontal gradient and tendency
in a NWP system: Dynamic QC. *J. Meteor. Soc. Japan*, **76**: 497-516.
- Oye R, Mueller C, Smith C, 1995. Software for radar data translation, visualization, editing,
and interpolation. *Preprints, 27th Conf. on Radar Meteorology, Vail, CO, Amer. Meteor.
Soc.*,: 359-361.
- Schaefer JT, 1990. The critical success index as an indicator of warning skill. *Wea. Forecasting*,
5: 570-575.
- Segami A, Kurihara K, Nakamura H, Ueno M, Takano I, Tatsumi Y, 1989. Operational
mesoscale weather prediction with Japan spectral model. *J. Meteor. Soc. Japan*, **67**: 907-
923.
- Song J-J, Wang Y, Wu L, 2010. Trend discrepancies among three best track data sets of western
North Pacific tropical cyclones. *J. Geophys. Res.*, **115**: D12128.
- Stern DP, Nolan DS, 2009. Reexamining the vertical structure of tangential winds in tropical
cyclones: Observations and theory. *J. Atmos. Sci.*, **66**: 3579-3600.
- Tsuyuki T, Fujita T, 2002: Outline of the Operational Numerical Weather Prediction at the
Japanese Meteorological Agency, JMA Report, 157pp.

- Wu L, Wang B, 2000. A potential vorticity tendency diagnostic approach for tropical cyclone motion. *Mon. Wea. Rev.*, **128**: 1899-1911.
- Wu L, Wang B, 2001. Movement and vertical coupling of adiabatic baroclinic tropical cyclones. *J. Atmos. Sci.*, **58**: 1801-1814.
- Xiao Q, Chen L, Zhang X, 2009. Evaluations of BDA scheme using the Advanced Research WRF (ARW) model. *J. App. Meteor. Climatology*, **48**: 680-689.
- Xiao Q, Kuo Y-H, Sun J, Lee W-C, Barker DM, Lim E, 2007. An approach of radar reflectivity data assimilation and its assessment with the inland QPF of typhoon Rusa (2002) at landfall. *J. Appl. Meteor. Climatology* **46**: 14-22.
- Xue M, Wang D-H, Gao J-D, Brewster K, Droegemeier KK, 2003. The Advanced Regional Prediction System (ARPS), storm-scale numerical weather prediction and data assimilation. *Meteor. Atmos. Physics*, **82**: 139-170.
- Xue M, Droegemeier KK, Wong V, Shapiro A, Brewster K, Carr F, Weber D, Liu Y, Wang D-H, 2001. The Advanced Regional Prediction System (ARPS) - A multiscale nonhydrostatic atmospheric simulation and prediction tool. Part II: Model physics and applications. *Meteor. Atmos. Phy.*, **76**: 143-165.
- Yu H, C. Hu, and L. Jiang, 2007. Comparison of three tropical cyclone intensity datasets. *Acta Meteorologica Sinica.*, **21**: 121 - 128.

- Zhang F, Weng Y, Sippel JA, Meng Z, Bishop CH, 2009. Cloud-resolving hurricane initialization and prediction through assimilation of Doppler radar observations with an ensemble Kalman filter. *Mon. Wea. Rev.*, **137**: 2105-2125.
- Zhao K, Xue M, 2009. Assimilation of coastal Doppler radar data with the ARPS 3DVAR and cloud analysis for the prediction of Hurricane Ike (2008). *Geophys. Res. Lett.*: doi:10.1029/2009GL038658.
- Zhao K, Lee WC, Jou BJD, 2008a. Single Doppler radar observation of the concentric eyewall in Typhoon Saomai, 2006, near landfall. *Geophys. Res. Lett.*, **35**: L07807, doi:10.1029/2007GL032773.
- Zhao Q, Jin Y, 2008. High-Resolution Radar Data Assimilation For Hurricane Isabel (2003) At Landfall. *Bull. Amer. Meteor. Soc.*, **89**: 1355-1372.
- Zhao Q, Cook J, Xu Q, Harasti PR, 2006. Using Radar Wind Observations to Improve Mesoscale Numerical Weather Prediction. *Wea. Forecasting*, **21**: 502-522.
- Zhao Q, Cook J, Xu Q, Harasti PR, 2008b. Improving Short-Term Storm Predictions by Assimilating both Radar Radial-Wind and Reflectivity Observations. *Wea. Forecasting*, **23**: 373-391.
- Zou X, Xiao Q, 2000. Studies on the Initialization and Simulation of a Mature Hurricane Using a Variational Bogus Data Assimilation Scheme. *J. Atmos. Sci.*, **57**: 836-860.

Table 1. Description of the radar data assimilation experiments

Experiments	Assimilation description
CNTL	No radar data assimilation
ExpGV	Assimilating GBVTD-retrieved winds, V_{GBVTD} (defined in Section 2)
ExpVr	Assimilating radial velocity data directly
ExpGVNoAsy	Same as ExpGV but without V_{Tn} , $n = 1,3$ component

List of figures

Fig. 1. The analysis and prediction domain at 3 km horizontal resolution, with the best track locations of super typhoon Saomai marked at 6-h intervals from 0000 UTC 9 to 1800 UTC 11 August, 2006. The locations of radar stations are shown by the black filled triangles and the ranges of the radar data coverage at WZRD are indicated by dashed circles for radial velocity and solid for reflectivity. The dashed rectangular box indicates the region of reflectivity/rainfall distribution in Fig. 13 and the reflectivity/rainfall verification. The gray shading shows the terrain height. Also shown are the province borders. Saomai made landfall near the border between Zhejiang Province to the north and Fujian Province to the south.

Fig. 2. Time-height plot of the root-mean-square errors between GBVTD-retrieved radial velocity and the observations from WZRD between 0400 UTC to 0600 UTC.

Fig. 3. The GBVTD analysis at 3 km height at 0400 (left column) and 0600 UTC (right column). From top to bottom are the GBVTD-retrieved winds (contours, unit in m s^{-1}) overlaid with observed reflectivity (upper panels), the observed Doppler radial velocity from WZRD (middle panels), and the radial velocity calculated from the GBVTD-retrieved winds (lower panels). Reflectivity is in color shades. The RMSE value of the retrieved radial velocity calculated against the observations is shown right corner in (e) and (f).

Fig. 4. Horizontal wind vectors and speed (color contours, m s^{-1}) at 3 km MSL, at 0400 UTC, the beginning time of the data assimilation window for (a) background forecast starting from JMA reanalysis at 0000 UTC, (b) the analysis from ExpVr using radial velocity data, and (c) the analysis from ExpGV using GBVTD-retrieved winds.

Fig. 5. Mean-sea-level pressure (MSLP, thick solid contours), and surface wind speed (color shaded contours, m s^{-1}) for typhoon Saomai at 0600 UTC 10 August 2006, from experiments (a) CNTL, (b) ExpVr, and (c) ExpGV. The black dot near the domain center indicates the approximate center location of observed typhoon.

Fig. 6. Horizontal wind speed (m s^{-1}) in the east-west vertical cross sections through the analyzed typhoon centers in Fig.5 for experiments (a) CNTL, (b) ExpVr, and (c) ExpGV.

Fig. 7. Analyzed azimuthal mean tangential winds (shaded with the scale on the right) at 0600 UTC 10 August 2006 from experiments (a) CNTL, (b) ExpVr, and (c) ExpGV. Dashed lines in (b) and (c) indicate the axis of RMW.

Fig. 8. Observed (1st row) and predicted (other rows) composite (column maximum)reflectivity and the wind vectors at 3km MSL corresponding to 3-h (0900 UTC, 1st column), 6-h (1200 UTC, 2nd column), 9-h (1500 UTC, 3rd column) and 12-h (1800 UTC, 4th column) forecasts, from experiments CNTL (2nd row), ExpVr (3rd row), and ExpGV (4th row).

Fig. 9. The 3-h forecasts of MSLP (thick solid contours), and surface wind speed (shaded contours, m s^{-1}) for typhoon Saomai at 0900 UTC 10 Aug 2006, from experiments (a) CNTL, (b) ExpVr, and (c) ExpGV. The black dot near the domain center indicates the approximate center location of observed typhoon.

Fig. 10. South-north vertical cross sections of 3-hour forecast equivalent potential temperature (solid contours at 2 K intervals) and horizontal wind speed (shaded contours, m s^{-1}) valid at 0900 UTC 10 Aug 2006 from experiments (a) CNTL, (b) ExpVr, and (c) ExpGV.

Fig. 11. Azimuthally averaged tangential wind (shaded with the scale on the right) and temperature deviation (solid isolines with interval of $2\text{ }^{\circ}\text{C}$) at 0900 UTC 10 Aug 2006 for experiments (a) CNTL, (b) ExpVr, and (c) ExpGV.

Fig. 12. The 12-h predicted (a) tracks, (b) track errors, (c) minimum MSLP (hPa) and (d) maximum surface wind speed (m s^{-1}) of super typhoon Saomai (2006) from 0600 UTC to 1800 UTC August 10 2006. Large dashed circle in (a) is the 150-km range ring for WZRD. The numbers in (b) represent the mean track errors over the 12-h forecast period. The labels in (a) and (d) are same as that in (c).

Fig. 13. Twelve-hour accumulated precipitation (mm) valid at 1800 UTC 10 August 2006 from (a) automatic weather station hourly observations, and experiments (b) CNTL, (c) ExpVr, and (d) ExpGV.

Fig. 14. (a) Equitable threat scores and (b) bias scores of the 12-h accumulated precipitation forecasts from CNTL, ExpVr, and ExpGV (shown in Fig. 13) verified against automatic weather station hourly observations (as shown in Fig. 13a) at 1800 UTC 10 August 2006.

Fig. 15. Equitable threat scores of predicted reflectivity for (a) 20-dBZ and (b) 40-dBZ threshold from experiments CNTL, ExpVr, and ExpGV, respectively.

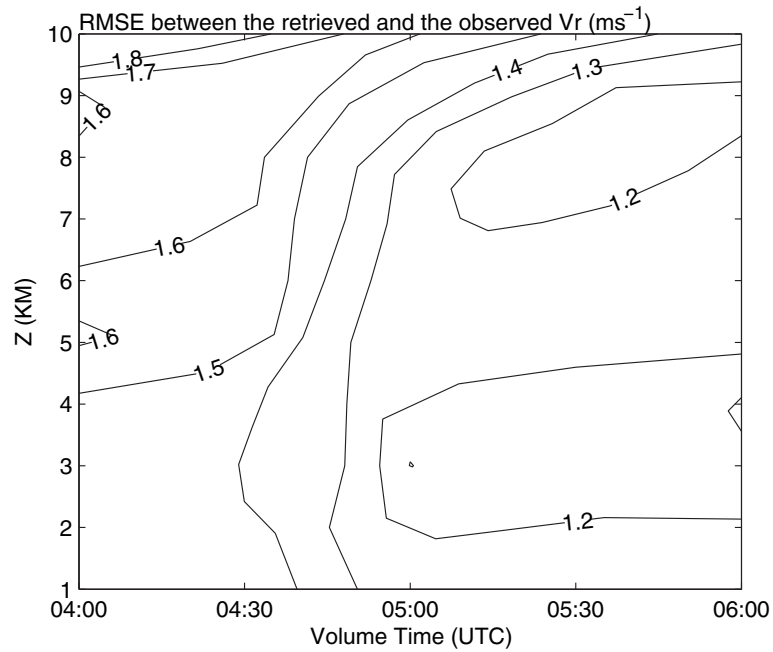


Fig. 2. Time-height plot of the root-mean-square errors between GBVTD-retrieved radial velocity and the observations from WZRD between 0400 UTC to 0600 UTC.

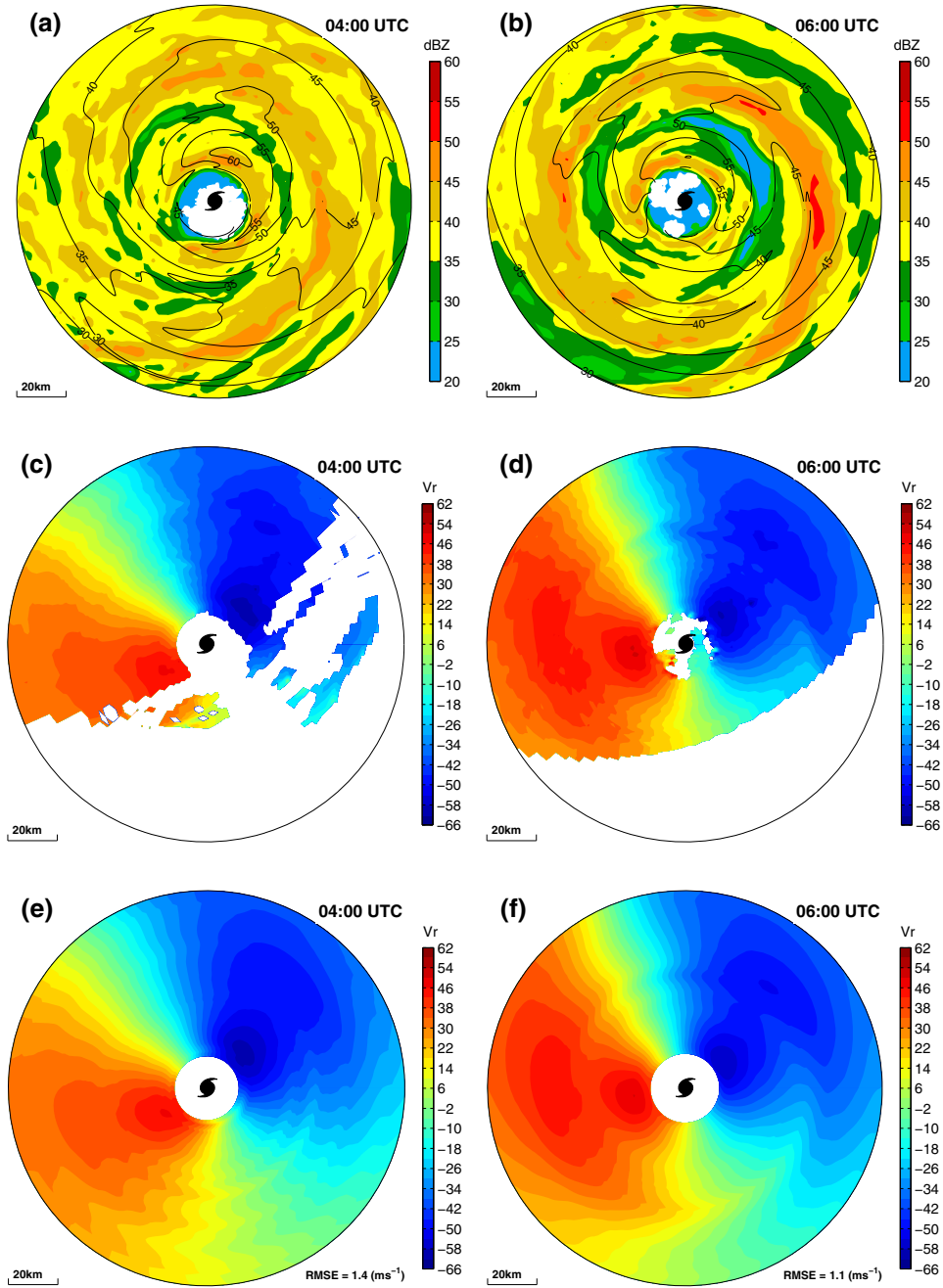


Fig. 3. The GBVTD analysis at 3 km height at 0400 (left column) and 0600 UTC (right column). From top to bottom are the GBVTD-retrieved winds (contours, unit in m s^{-1}) overlaid with observed reflectivity (upper panels), the observed Doppler radial velocity from WZRD (middle panels), and the radial velocity calculated from the GBVTD-retrieved winds (lower panels). Reflectivity is in color shades. The RMSE value of the retrieved radial velocity calculated against the observations is shown right corner in (e) and (f).

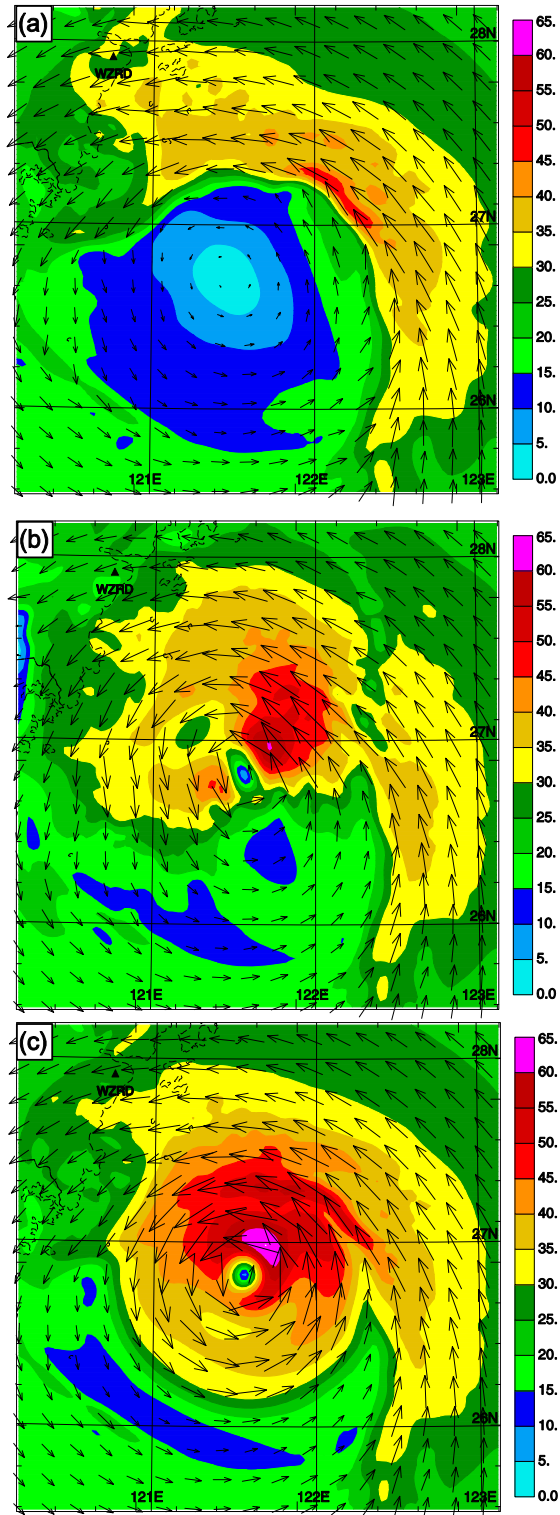


Fig. 4. Horizontal wind vectors and speed (color contours, m s^{-1}) at 3 km MSL, at 0400 UTC, the beginning time of the data assimilation window for (a) background forecast starting from JMA reanalysis at 0000 UTC, (b) the analysis from ExpVr using radial velocity data, and (c) the analysis from ExpGV using GBVTD-retrieved winds.

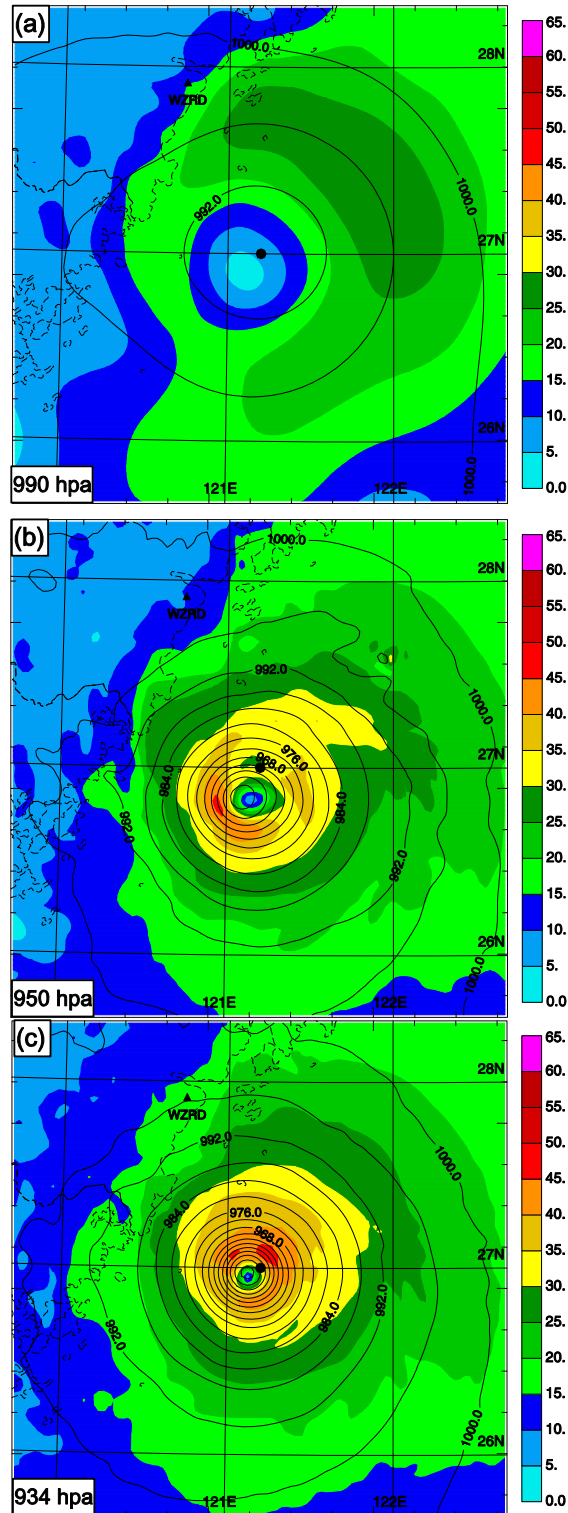


Fig. 5. Mean-sea-level pressure (MSLP, thick solid contours), and surface wind speed (color shaded contours, m s^{-1}) for typhoon Saomai at 0600 UTC 10 August 2006, from experiments (a) CNTL, (b) ExpVr, and (c) ExpGV. The black dot near the domain center indicates the approximate center location of observed typhoon.

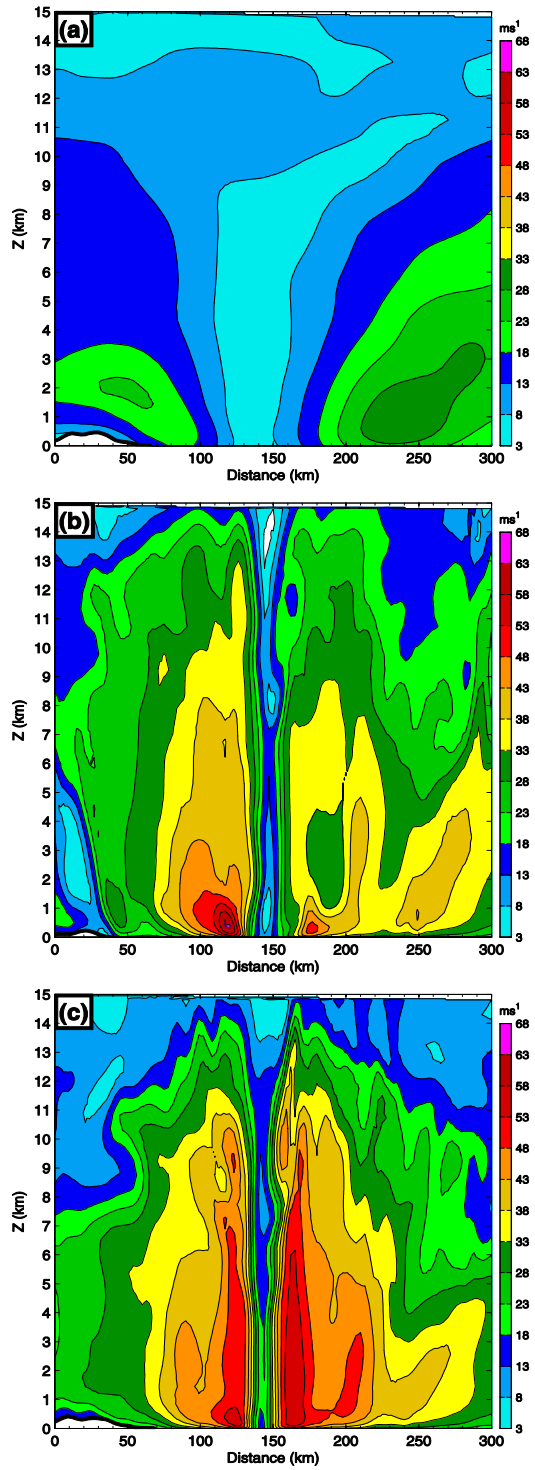


Fig. 6. Horizontal wind speed (m s^{-1}) in the east-west vertical cross sections through the analyzed typhoon centers in Fig.5 for experiments (a) CNTL, (b) ExpVr, and (c) ExpGV.

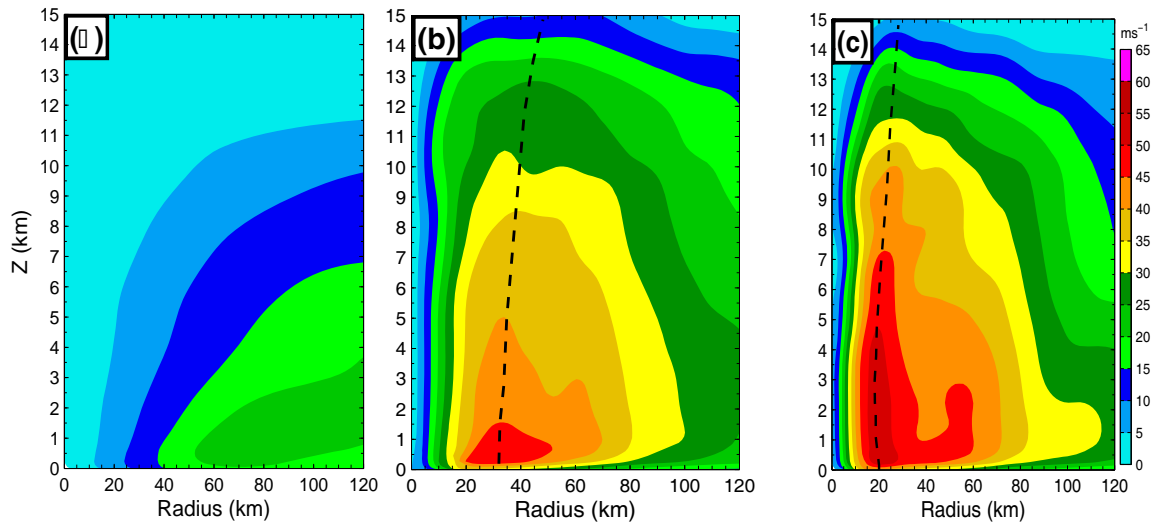


Fig. 7. Analyzed azimuthal mean tangential winds (shaded with the scale on the right) at 0600 UTC 10 August 2006 from experiments (a) CNTL, (b) ExpVr, and (c) ExpGV. Dashed lines in (b) and (c) indicate the axis of RMW.

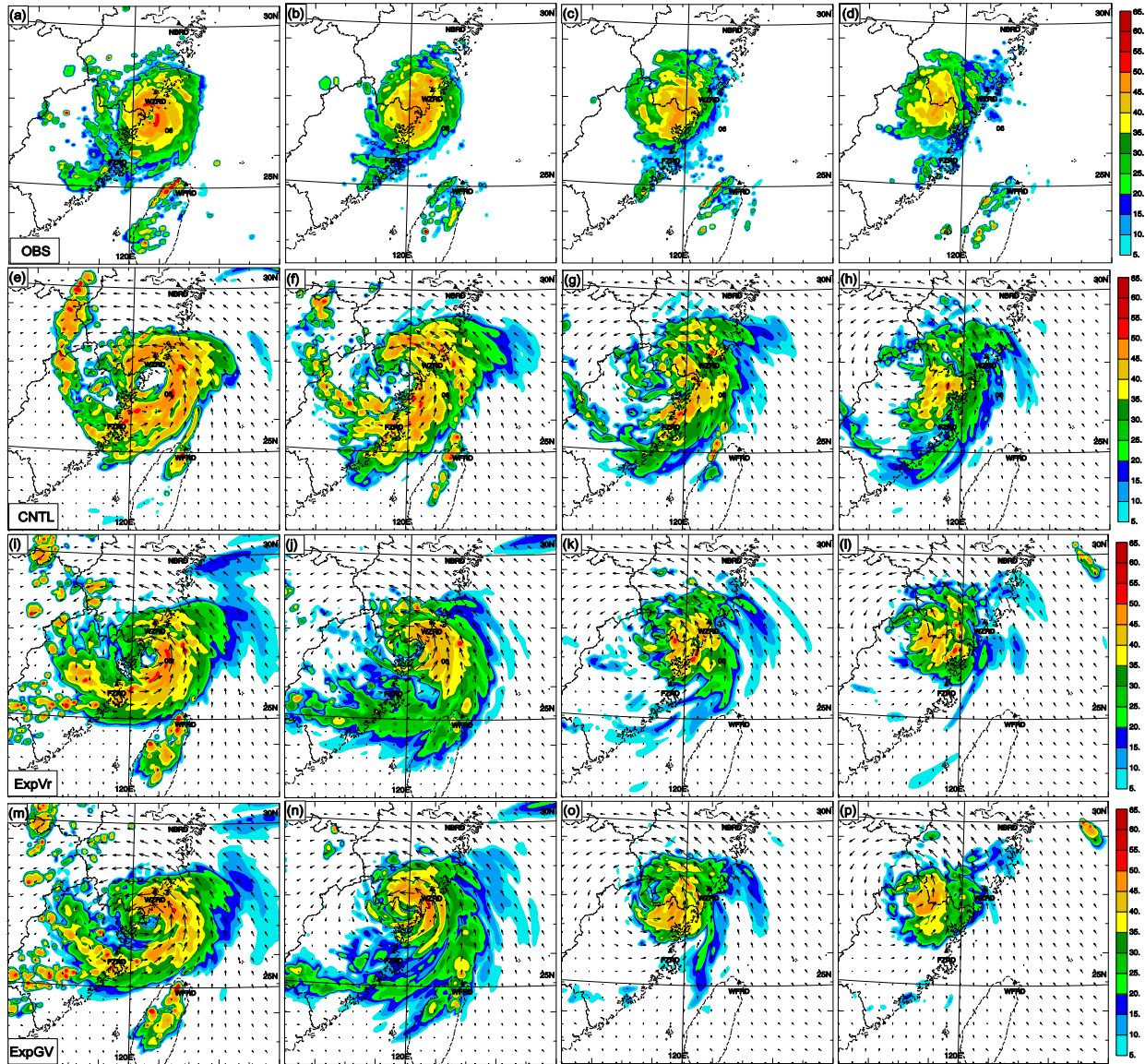


Fig. 8. Observed (1st row) and predicted (other rows) composite (column maximum)reflectivity and the wind vectors at 3km MSL corresponding to 3-h (0900 UTC, 1st column), 6-h (1200 UTC, 2nd column), 9-h (1500 UTC, 3rd column) and 12-h (1800 UTC, 4th column) forecasts, from experiments CNTL (2nd row), ExpVr (3rd row), and ExpGV (4th row).

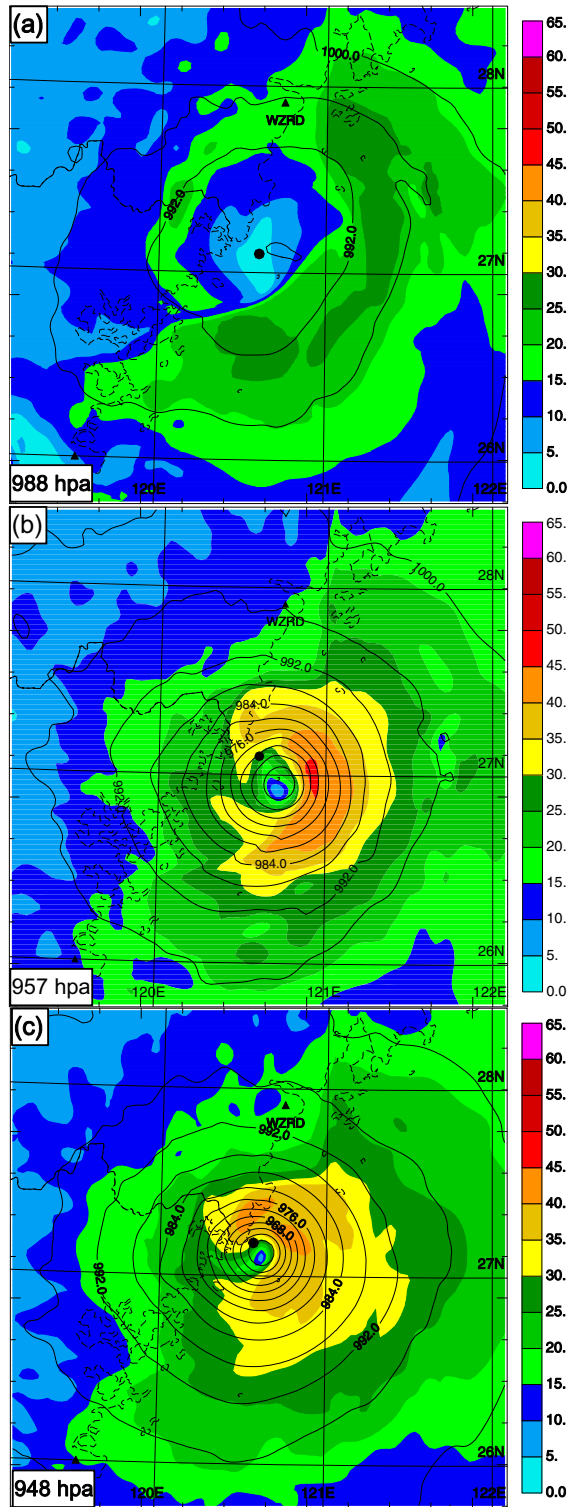


Fig. 9. The 3-h forecasts of MSLP (thick solid contours), and surface wind speed (shaded contours, m s^{-1}) for typhoon Saomai at 0900 UTC 10 Aug 2006, from experiments (a) CNTL, (b) ExpVr, and (c) ExpGV. The black dot near the domain center indicates the approximate center location of observed typhoon.

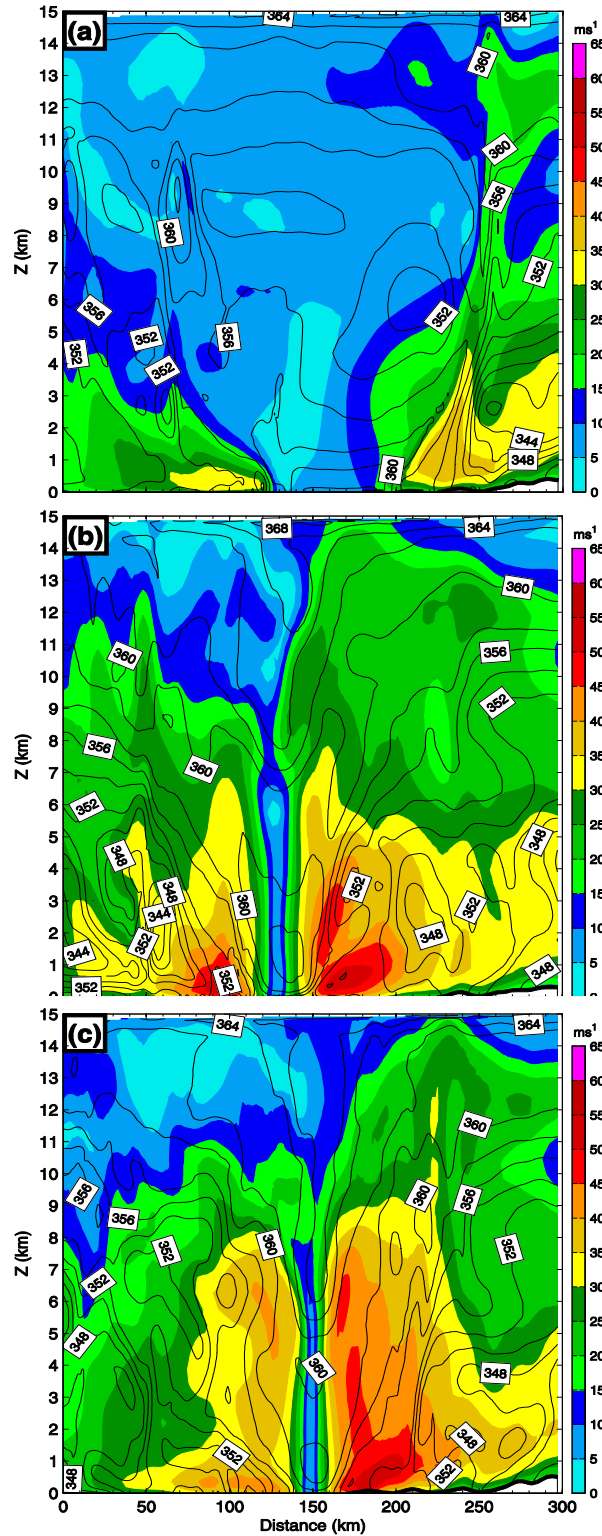


Fig. 10. South-north vertical cross sections of 3-hour forecast equivalent potential temperature (solid contours at 2 K intervals) and horizontal wind speed (shaded contours, m s^{-1}) valid at 0900 UTC 10 Aug 2006 from experiments (a) CNTL, (b) ExpVr, and (c) ExpGV.

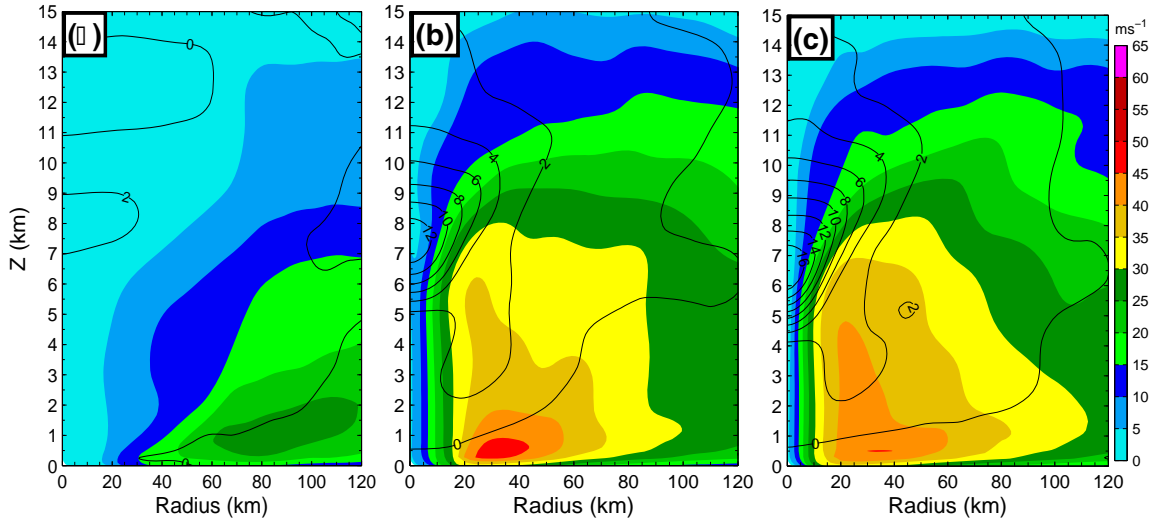


Fig. 11. Azimuthally averaged tangential wind (shaded with the scale on the right) and temperature deviation (solid isolines with interval of 2 $^{\circ}\text{C}$) at 0900 UTC 10 Aug 2006 for experiments (a) CNTL, (b) ExpVr, and (c) ExpGV.

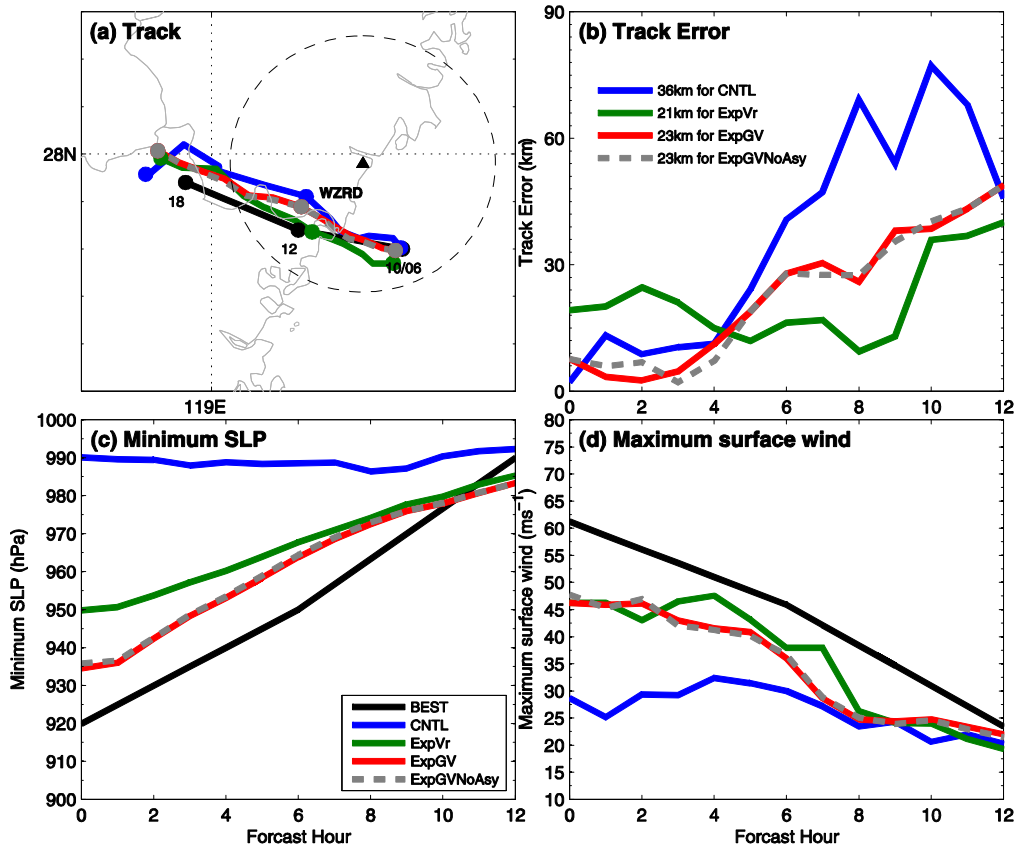


Fig. 12. The 12-h predicted (a) tracks, (b) track errors, (c) minimum MSLP (hPa) and (d) maximum surface wind speed (m s^{-1}) of super typhoon Saomai (2006) from 0600 UTC to 1800 UTC August 10 2006. Large dashed circle in (a) is the 150-km range ring for WZRD. The numbers in (b) represent the mean track errors over the 12-h forecast period. The labels in (a) and (d) are same as that in (c).

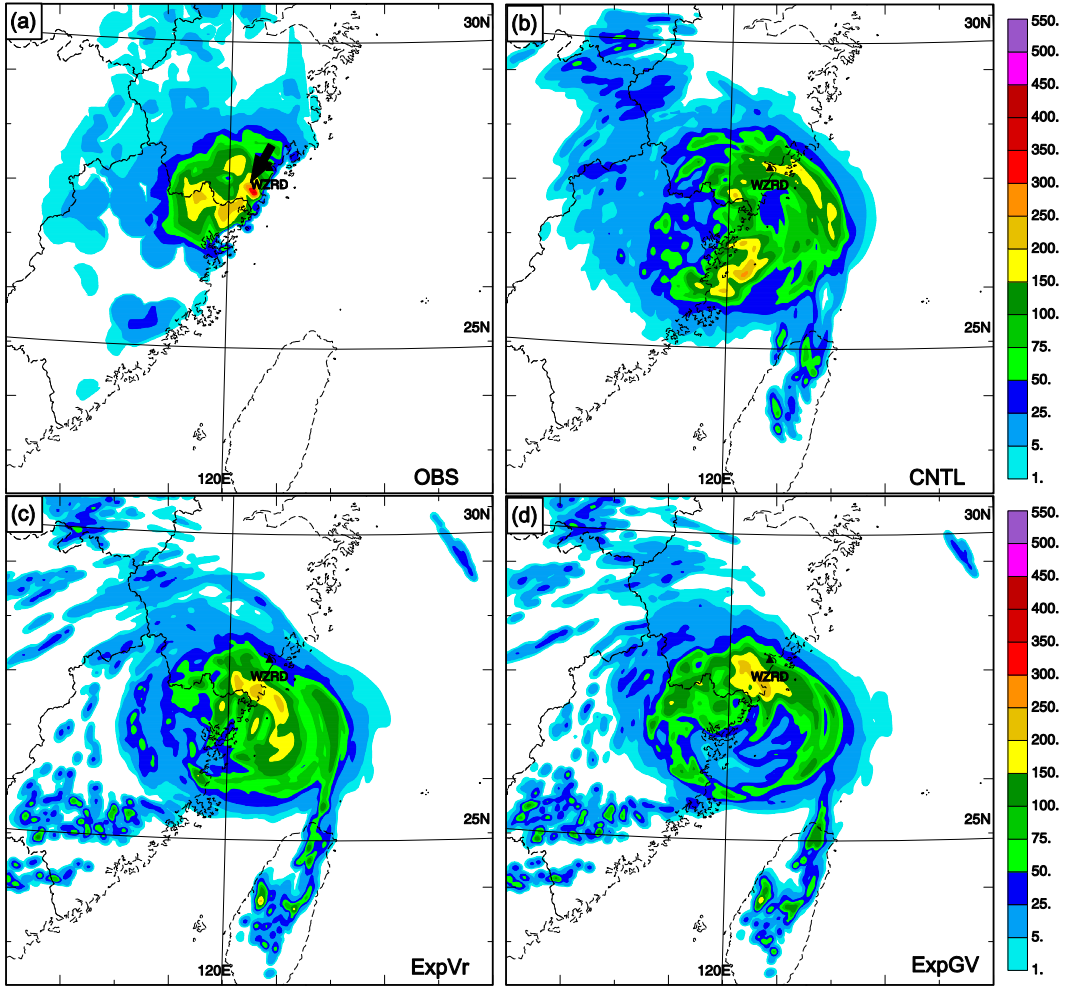


Fig. 13. Twelve-hour accumulated precipitation (mm) valid at 1800 UTC 10 August 2006 from (a) automatic weather station hourly observations, and experiments (b) CNTL, (c) ExpVr, and (d) ExpGV.

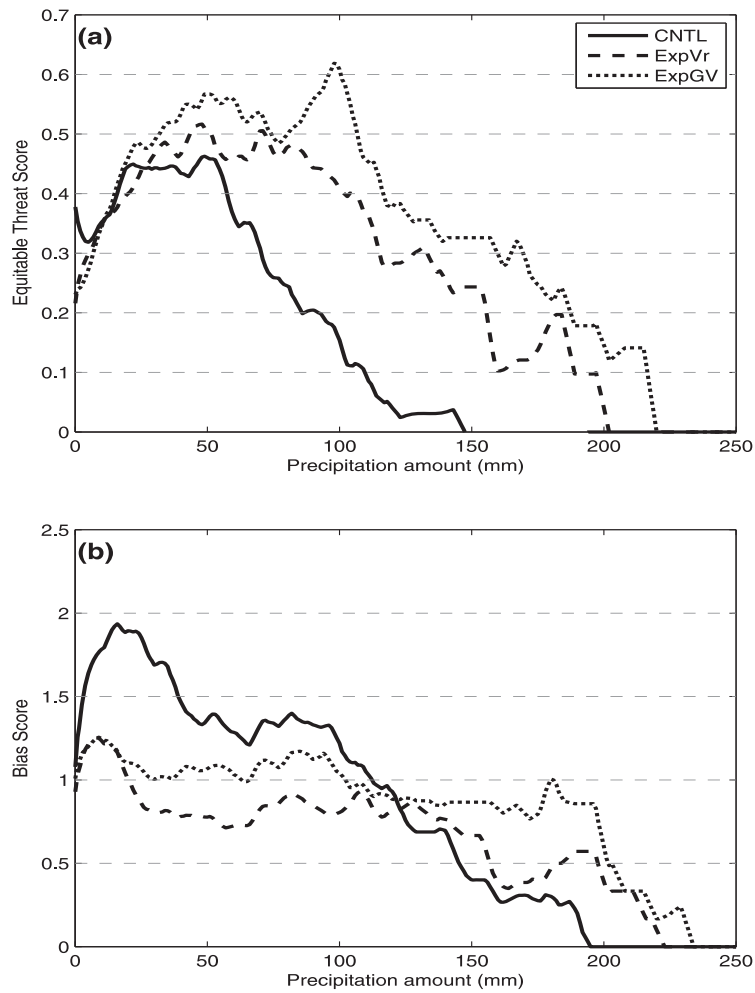


Fig. 14. (a) Equitable threat scores and (b) bias scores of the 12-h accumulated precipitation forecasts from CNTL, ExpVr, and ExpGV (shown in Fig. 13) verified against automatic weather station hourly observations (as shown in Fig. 13a) at 1800 UTC 10 August 2006.

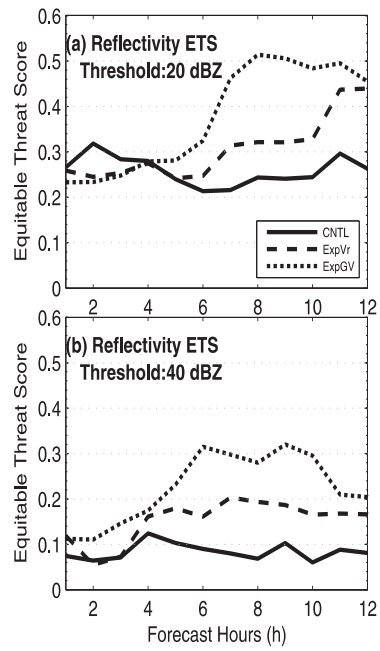


Fig. 15. Equitable threat scores of predicted reflectivity for (a) 20-dBZ and (b) 40-dBZ threshold from experiments CNTL, ExpVr, and ExpGV, respectively.